Theory of Metamaterial Beams for Broadband Vibration Absorption

HONGWEI SUN,[1] XINGWEN DU[1] AND P. FRANK PAI[2,*]

[1]*Center for Composite Materials and Structures, Harbin Institute of Technology, Harbin 150001, China*

[2]*Department of Mechanical and Aerospace Engineering, University of Missouri, Columbia, MO 65211, USA*

ABSTRACT: This article presents methods for modeling, analysis, and design of metamaterial beams for broadband vibration absorption/isolation. The proposed metamaterial beam consists of a uniform isotropic beam with many small spring-mass-damper subsystems integrated at separated locations along the beam to act as vibration absorbers. For a unit cell of an infinite metamaterial beam, governing equations are derived using the extended Hamilton principle. The existence of stopband is demonstrated using a model based on averaging material properties over a cell length and a model based on finite element modeling and the Bloch–Floquet theory for periodic structures. However, these two idealized models cannot be used for finite beams and/or elastic waves having short wavelengths. For finite metamaterial beams, a linear finite element method is used for detailed modeling and analysis. Both translational and rotational absorbers are considered. Because results show that rotational absorbers are not efficient, only translational absorbers are recommended for practical designs. The concepts of negative effective mass and stiffness and how the spring-mass-damper subsystems create a stopband (i.e., no elastic waves in this frequency range can propagate forward) are explained in detail. Numerical simulations reveal that the actual working mechanism of the proposed metamaterial beam is based on the concept of conventional mechanical vibration absorbers. It uses the incoming elastic wave in the beam to resonate the integrated spring-mass-damper absorbers to vibrate in their optical mode at frequencies close to but above their local resonance frequencies to create shear forces and bending moments to straighten the beam and stop the wave propagation. This concept can be easily extended to design a broadband absorber that works for elastic waves of short and long wavelengths. Numerical examples validate the concept and show that, for high-frequency waves, the structure's boundary conditions do not have significant influence on the absorbers' function. However, for absorption of low-frequency waves, the boundary conditions and resonant modes of the structure need to be considered in the design. With appropriate design calculations, finite discrete spring-mass-damper absorbers can be used, and hence expensive micro- or nanomanufacturing techniques are not needed for design and manufacturing of such metamaterial beams for broadband vibration absorption/isolation.

Key Words: acoustic metamaterial beams, stopband, broadband vibration isolation, negative effective mass and stiffness, local mechanical resonance, periodic structures, phononic structures.

INTRODUCTION

METAMATERIALS are a new class of composites proposed in 2001 by the Defense Advanced Research Projects Agency (DARPA) to exhibit exceptional material properties not observed in nature or in the constituent materials in order to develop new technologies (Chen, 2005; Liu, 2005; Sachan and Majetich, 2005). The transcendental properties of metamaterials are assumed to arise from their engineered constructs using artificially fabricated, extrinsic, low-dimensional inhomogeneities. This concept gives engineers a license to dream and think out of the constraints imposed by the performance limitations of conventional materials.

Electromagnetic Metamaterials

Metamaterials were first introduced for dealing with electromagnetic waves (Pendry, 2000, 2004; Chen, 2005; Liu, 2005; Sachan and Majetich, 2005; Tanaka et al., 2006; Tanaka, 2008). The four material parameters intrinsic to magnetoelectric coupling of bi-isotropic

*Author to whom correspondence should be addressed.
E-mail: paip@missouri.edu
Figures 1–13 appear in color online: http://jim.sagepub.com

1045-389X/10/11 1085–17 $10.00/0 DOI: 10.1177/1045389X10375637

media are the permittivity ε, permeability μ, strength of chirality κ, and Tellegen parameter χ, and they interact with the electric field strength **E**, magnetic field strength **H**, electric flux density **D**, and magnetic flux density **B**. A material is made of atoms that are dipoles, and these dipoles modify the velocity of an electromagnetic wave coming into the material by a factor $n\,(\equiv \pm\sqrt{\varepsilon\mu}$, the refractive index). When an electromagnetic wave enters a material, its electric and magnetic fields interact/resonate with the material's electrons and other charges, and the charges are driven to oscillate and radiate their own electromagnetic wave that has the same frequency but a different phase. The macroscopic sum of all such contributions in the material is a wave having the same frequency but a wavelength shorter than the original one, leading to a decrease or even reverse of the wave's phase velocity. Waves propagate in the forward direction if $\varepsilon > 0$ and $\mu > 0$, in the backward direction if $\varepsilon < 0$ and $\mu < 0$, and no wave propagation if $\varepsilon\mu < 0$ (Veselago, 1968). For a metamaterial with $n < 0$, its electric field, magnetic field, and wave vector follow a left-hand rule and it is called a left-handed material. κ and χ affect a wave's phase. In bi-isotropic media with $\kappa \neq 0$ and $\chi = 0$, a backward wave plus a forward wave can occur, and two forward waves or two backward waves can also occur, depending on the value of κ. If $\kappa > \sqrt{\varepsilon\mu}$, metamaterials with $n < 0$ can be manufactured.

The optical resonance between an electromagnetic wave and a material's charges has been used to design metamaterials with $\varepsilon < 0$ and $\mu < 0$, and hence, $n = -\sqrt{\varepsilon\mu} < 0$ (Pendry, 2000, 2004). Metamaterials with $n < 0$ have numerous startling properties: (1) It follows from Snell's law that rays will be refracted to the *same* side of the contacting surface's normal when entering a material. (2) The Doppler shift is reversed, that is, a light source moving toward an observer appears to reduce its frequency. (3) Cherenkov radiation points the other way. (4) The time-averaged Poynting vector is antiparallel to the phase velocity, and hence, the wave front is moving in a direction opposite to the direction of energy flow. Metamaterials with $n < 0$ can be used to design electromagnetic absorbers (i.e., cloaking devices) for rendering objects invisible and optical superlens for capturing images with a resolution many times smaller than the diffraction limit of conventional lenses. These two developments enable many new optical technologies (Pendry, 2004; Pendry et al., 2006; Schurig et al., 2006; Tanaka et al., 2006; Tanaka, 2008).

A material having either (but not both) $\varepsilon < 0$ or $\mu < 0$ is opaque to electromagnetic radiation. Although the optical properties of a transparent material are fully specified by ε and μ, the refractive index $n\,(\equiv \pm\sqrt{\varepsilon\mu})$ is often used in practice. All known natural transparent materials possess positive ε and μ, but many metals (e.g., silver and gold) have negative ε at visible wavelengths. Because natural materials do not have $\mu < 0$ and they only interact with a visible light's electric field, their relative permeability is fixed at unity. Hence, the challenge is how to design and manufacture metamaterials with $\mu < 0$. It was demonstrated that a split ring (C shape) with its axis placed along the direction of wave propagation could provide a negative permeability, and a periodic array of thin wires and rings could give rise to a negative refractive index (Pendry, 2000, 2004; Pendry et al., 2006). The thin wire acts as a ferroelectric atom, the ring acts as an inductor L, and the open section of the ring acts as a capacitor C. Hence, this split-ring resonator acts as an LC circuit, and the ring-wire units play the role of atomic dipoles. When an electromagnetic wave passes through the ring, a current is induced in the ring and the generated field is perpendicular to the wave's magnetic field. This magnetic resonance results in a negative macroscopic permeability. Metamaterials with negative diffractive indices have been demonstrated for microwave frequencies (in the gigahertz range with a wavelength of a few centimeters) and infrared frequencies (in the terahertz range with a wavelength about a human hair [17–181 μm]) (Pendry et al., 2006; Schurig et al., 2006). The ring-wire units can be replaced with electrically conductive units (e.g., loops of wire) that have suitable inductive and capacitive characteristics. However, all these units need to be much smaller than the wave's wavelength in order for these designs to work. Unfortunately, because the wavelength of visible light is short (400–700 nm), difficulties reside in how to manufacture subunits of such nanoscale sizes. Moreover, because metamaterials with $\varepsilon < 0$ and $\mu < 0$ are innately dispersive, their ε, μ, and n change with frequency.

An object emits propagating and non-propagating (evanescent) electromagnetic waves. Conventional lenses of positive refractive indices for far-field imaging systems (e.g., cameras) create images by capturing, refracting, and refocusing the propagating waves. Evanescent waves contain sub-wavelength details of the object, but they decay exponentially within the near field and never reach the image plane, resulting in the so-called diffraction limit. Hence, the finest feature size that can be resolved is on the order of one-half of the incident illuminating wavelength. An electromagnetic wave that reaches the surface of a lens having a negative refractive index excites a collective electric movement of surface waves (called surface plasmons) and hence amplify and restore the evanescent waves, resulting in images with a sub-diffraction-limited resolution. The surface plasmon resonance is a physical phenomenon that occurs when a light is coupled to a thin layer of metal (e.g., silver or gold) under certain angle of incidence, wavelength, polarization, and metal thickness.

Electromagnetic metamaterials are mainly designed by using the effects of negative refractive indices,

cloaking, and superlensing, which are in turn caused by designed optical resonance. Possible applications include optical fibers with no transmission loss, very thin optical lenses, radar lenses with compact and relatively aberration free performance, electromagnetic absorbers, technologies for rendering objects invisible, optical microscopes capable of observing atoms, subwavelength waveguides, photon tunneling, smaller antenna, backward wave antennae, artificial magnetic device composed of non-magnetic materials, high-performance permanent magnets, photolithography and nanolithography to make higher density electronic circuits, faster fiber-optic communications, detailed biomedical imaging in real time and *in vivo*, and visualizing proteins in intact cells using optical microscopes instead of a more complicated method like X-ray crystallography (Chen, 2005; Liu, 2005; Sachan and Majetich, 2005). For example, current optical microscopes can only resolve objects down to around 400 nm, which is about one-tenth the diameter of a red blood cell. In contrast, optical superlens having negative refractive indices can image nanoscale structures with a resolution that is about one-sixth the wavelength of light (Fang et al., 2005).

Acoustic Metamaterials

Recently, the analogy between electromagnetic and acoustic waves stimulates development of metamaterials for dealing with mechanical waves (Li and Chan, 2004; Milton and Willis, 2007; Wu et al., 2007; Cheng et al., 2008; Huang et al., 2009). For electromagnetic waves having wavelengths much longer than the distance between atoms, a material is well described by its locally averaged electromagnetic properties ε (permittivity) and μ (permeability). Similarly, for elastic waves having wavelengths much longer than the distance between atoms, a material can be treated as a continuum and is well described by its locally averaged mechanical properties E (Young's modulus) and ρ (mass density). The transcendental properties (e.g., $\mu < 0$, $n < 0$, or $\mu \gg 1$) of an electromagnetic metamaterial mainly comes from the optical resonance between an electromagnetic wave and the material's man-made subunits. Similarly, acoustic metamaterials can be designed by building mechanical subunits in a natural material to resonate with mechanical waves propagating in it. Similar to the interaction between an electromagnetic wave and a material's charges, an elastic wave in a structure may resonate with the structure's subunits. This local mechanical resonance can be used to design acoustic metamaterials with negative effective mass and stiffness (Cheng et al., 2008; Yao et al., 2008).

Acoustic metamaterials are designed by building subunits to create the desired, averaged, non-natural material properties. In the literature, only few simple models for bar-like acoustic metamaterials were proposed, and they are all based on spatial averaging of heterogeneous material properties and hence are valid only for waves of wavelengths much longer than the sizes of subunits (Li and Chan, 2004; Milton and Willis, 2007; Wu et al., 2007; Cheng et al., 2008; Yao et al., 2008; Huang et al., 2009). If a metamaterial is to behave like a homogeneous material described by its averaged material properties, its subunits must be much smaller than the shortest wavelength of waves propagating in it. The averaging may result in the existence of a useful but mysterious phononic stopband that allows no waves within that frequency range to propagate forward, and most current designs of acoustic metamaterials are based on the stopband effect (Huang et al., 2009). To manufacture such metamaterials with tiny subunits in order to have stopbands, expensive manufacturing techniques are required, including micro- and nanomanufacturing techniques that are still under development.

Similar to electromagnetic metamaterials, acoustic metamaterials may enable development of many new technologies, including acoustic absorbers using the stopband effect, acoustic imaging below the diffraction limit using the superlensing effect, super environmental acoustic absorbers, and subwavelength waveguides. However, theoretical development for acoustic metamaterials is a great challenge, and appropriate modeling and design of such built-up structures are other difficulties.

Objectives

This work is to perform theoretical development and numerical validation for a new class of metamaterial beams for broadband absorption/isolation of transverse elastic waves. The specific objectives are (1) to develop appropriate modeling and analysis methods and demonstrate cloaking of elastic waves in a beam with integrated spring-mass subsystems as shown in Figure 1, (2) to reveal the actual working mechanism of metamaterial beams for absorption of low- and high-frequency elastic waves, and (3) to design and numerically verify a broadband elastic wave absorber that does not require micro- or nanomanufacturing techniques.

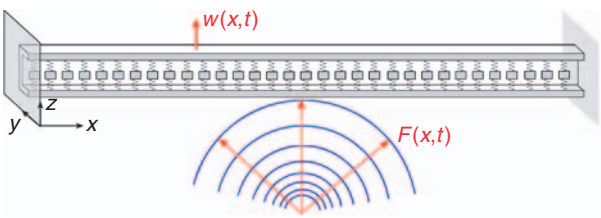

Figure 1. *A metamaterial beam for vibration absorption/isolation.*

NEGATIVE EFFECTIVE MATERIAL PROPERTIES

Negative Effective Mass

To demonstrate the concepts of negative effective mass and vibration absorbers, we consider the two-degree-of-freedom (2-DOF) mass-in-mass system shown in Figure 2(a) subjected to a harmonic excitation. The equations of motion, frequency response functions (FRFs) H_{i1} (Ω) $(i=1, 2)$ between the response $u_i(t)$ and the input harmonic force $F(t)$, and the effective mass $\tilde{m}_1(\Omega)$ are derived to be:

$$\begin{bmatrix} m_1 & 0 \\ 0 & m_2 \end{bmatrix}\begin{Bmatrix} \ddot{u}_1 \\ \ddot{u}_2 \end{Bmatrix}+\begin{bmatrix} k_2 & -k_2 \\ -k_2 & k_2 \end{bmatrix}\begin{Bmatrix} u_1 \\ u_2 \end{Bmatrix}=\begin{Bmatrix} F \\ 0 \end{Bmatrix},$$

$$F \equiv F_0 e^{j\Omega t}, \begin{Bmatrix} u_1 \\ u_2 \end{Bmatrix} \equiv \begin{Bmatrix} a_1 \\ a_2 \end{Bmatrix} e^{j\Omega t}$$

$$H_{11} \equiv \frac{a_1}{F_0} = \frac{k_2 - m_2\Omega^2}{(k_2 - m_1\Omega^2)(k_2 - m_2\Omega^2) - k_2^2}, \tag{1}$$

$$H_{21} \equiv \frac{a_2}{F_0} = \frac{k_2}{(k_2 - m_1\Omega^2)(k_2 - m_2\Omega^2) - k_2^2},$$

$$\tilde{m}_1 \equiv \frac{F}{\ddot{u}_1} = \frac{F_0}{-\Omega^2 a_1} = m_1 + \frac{m_2}{1 - \Omega^2/\omega_2^2}, \quad \omega_2 \equiv \sqrt{\frac{k_2}{m_2}}$$

where $j \equiv \sqrt{-1}$, $\dot{u}_1 \equiv \mathrm{d}u_1/\mathrm{d}t$, t is time, Ω is the excitation frequency, and ω_2 is the local resonance frequency of the spring-mass vibration absorber (consisting of m_2 and k_2). The effective mass $\tilde{m}_1$ is defined by treating this 2-DOF system as a 1-DOF system by assuming the internal absorber being unknown to the observer. If $\Omega = \omega_2$, Equation (1) shows that $|\tilde{m}| \to \infty$, $H_{11} = u_1 = 0$, $F_0 = -k_2 a_2$, and $F(t) = -k_2 u_2(t) = m_2 \ddot{u}_2(t)$. In other words, the external force is cancelled out by the inertia force $-m_2\ddot{u}_2$ through the spring k_2, and hence, $u_1(t) = 0$, and this is the key concept of mechanical vibration absorbers. This also reveals that for a specified harmonic excitation with $\Omega = \omega_2$, $a_2 (= -F_0/k_2 = -F_0/(m_2\Omega^2))$ increases when m_2 decreases. Moreover, when $\Omega > \omega_2$ and $m_2/(\Omega^2/\omega_2^2 - 1) > m_1$, the effective mass $\tilde{m}$ becomes negative.

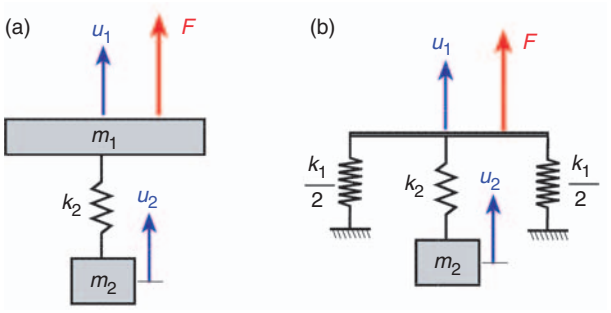

Figure 2. *Two-DOF systems: (a) mass-in-mass, and (b) mass-in-spring.*

If $\Omega < \omega_2$, because $\tilde{m}_1 > 0$, $F_0/a_1 = -\tilde{m}_1\Omega^2 < 0$, and $F_0/a_2 = \tilde{m}_1\Omega^2(\Omega^2/\omega_2^2 - 1) < 0$, $u_1(t)$ and $u_2(t)$ are in phase, and the vibration pattern is called an acoustic mode. If $\Omega > \omega_2$ and $\tilde{m}_1 < 0$, because $F_0/a_1 = -\tilde{m}_1\Omega^2 > 0$ and $F_0/a_2 = \tilde{m}_1\Omega^2(\Omega^2/\omega_2^2 - 1) < 0$, $u_1(t)$ and $u_2(t)$ are 180° out of phase, and the vibration pattern is called an optical mode. If $\Omega > \omega_2$ and $\tilde{m}_1 > 0$, because $F_0/a_1 = -\tilde{m}_1\Omega^2 < 0$ and $F_0/a_2 = \tilde{m}_1\Omega^2(\Omega^2/\omega_2^2 - 1) > 0$, $u_1(t)$ and $u_2(t)$ are 180° out of phase, and it is also an optical mode. When $\Omega > \omega_2$ and $\tilde{m}_1 < 0$, the downward pulling spring force on m_1 is $k_2(a_1 - a_2) = F_0(\tilde{m}_1 - m_1)/\tilde{m}_1 > F_0$, which is why the effective mass $\tilde{m}_1$ becomes negative.

Negative Effective Stiffness

To demonstrate the concept of negative effective stiffness, we consider the 2-DOF mass-in-spring system shown in Figure 2(b). The equations of motion, FRF H_{i1} (Ω) $(i=1, 2)$ between the response $u_i(t)$ and the input harmonic force $F(t)$, and the effective stiffness $\tilde{k}_1(\Omega)$are derived to be:

$$\begin{bmatrix} 0 & 0 \\ 0 & m_2 \end{bmatrix}\begin{Bmatrix} \ddot{u}_1 \\ \ddot{u}_2 \end{Bmatrix}+\begin{bmatrix} k_1 + k_2 & -k_2 \\ -k_2 & k_2 \end{bmatrix}\begin{Bmatrix} u_1 \\ u_2 \end{Bmatrix}=\begin{Bmatrix} F \\ 0 \end{Bmatrix},$$

$$F \equiv F_0 e^{j\Omega t}, \begin{Bmatrix} u_1 \\ u_2 \end{Bmatrix} \equiv \begin{Bmatrix} a_1 \\ a_2 \end{Bmatrix} e^{j\Omega t}$$

$$H_{11} \equiv \frac{a_1}{F_0} = \frac{k_2 - m_2\Omega^2}{(k_1 + k_2)(k_2 - m_2\Omega^2) - k_2^2} = \frac{1}{\tilde{k}_1}, \tag{2}$$

$$H_{21} \equiv \frac{a_2}{F_0} = \frac{k_2}{(k_1 + k_2)(k_2 - m_2\Omega^2) - k_2^2}$$

$$\tilde{k}_1 \equiv \frac{F}{u_1} = \frac{F_0}{a_1} = k_1 + \frac{k_2}{1 - \omega_2^2/\Omega^2}, \quad \omega_2 \equiv \sqrt{\frac{k_2}{m_2}}$$

The effective stiffness $\tilde{k}_1$ is defined by treating this 2-DOF system as a 1-DOF system by assuming the internal absorber being unknown to the observer. If $\Omega = \omega_2$, Equation (2) shows that $|\tilde{k}_1| \to \infty$, $H_{11} = u_1 = 0$, $F_0 = -k_2 a_2$, and $F(t) = -k_2 u_2(t) = m_2 \ddot{u}_2(t)$. In other words, the external force is cancelled out by the inertia force $-m_2\ddot{u}_2$ through the spring k_2, and hence, $u_1(t) = 0$, and this is the key concept of mechanical vibration absorbers. This also reveals that for a specific harmonic excitation with $\Omega = \omega_2$, $a_2 (= -F_0/k_2 = -F_0/(m_2\Omega^2))$ increases when m_2 decreases. Moreover, when $\Omega < \omega_2$ and $k_2/(\omega_2^2/\Omega^2 - 1) > k_1$, the effective stiffness $\tilde{k}_1$ becomes negative.

If $\Omega < \omega_2$ and $\tilde{k}_1 > 0$, because $F_0/a_1 = \tilde{k}_1 > 0$ and $F_0/a_2 = \tilde{k}_1(1 - \Omega^2/\omega_2^2) > 0$, motions of $u_1(t)$ and $u_2(t)$ are in phase, and it is an acoustic mode. If $\Omega < \omega_2$ and $\tilde{k}_1 < 0$, because $F_0/a_1 = \tilde{k}_1 < 0$ and $F_0/a_2 = \tilde{k}_1(1 - \Omega^2/\omega_2^2) < 0$, motions of $u_1(t)$ and $u_2(t)$ are in phase, and it is also an acoustic mode. If $\Omega > \omega_2$, because

$\tilde{k}_1 > 0$, $F_0/a_1 = \tilde{k}_1 > 0$, and $F_0/a_2 = \tilde{k}_1(1 - \Omega^2/\omega_2^2) < 0$, motions of $u_1(t)$ and $u_2(t)$ are 180° out of phase, and it is an optical mode. When $\Omega < \omega_2$ and $\tilde{k}_1 < 0$, the downward pulling spring force against $F(t)$ is $k_2(a_1 - a_2) = F_0(\tilde{k}_1 - k_1)/\tilde{k}_1 > F_0$, which explains why the effective stiffness $\tilde{k}_1$ is negative.

Discussions

Figure 2(a) and Equation (1) show that the translational vibration absorber can work efficiently, in an optical mode, against an external force acting on a mass with $\Omega > \omega_2$. On the other hand, Figure 2(b) and Equation (2) show that the translational vibration absorber can work efficiently, in an acoustic mode, against an external force acting on a spring with $\Omega < \omega_2$. Unfortunately, a beam has both mass and spring effects, and transverse elastic waves in beams are dispersive, that is, waves of different wavelengths propagate at different speeds.

Transverse waves propagate in a beam through internal shear forces and bending moments. Hence, both translational and rotational vibration absorbers may need to be considered for use in order to efficiently prevent waves from propagating forward.

GOVERNING EQUATIONS OF A BEAM-LIKE VIBRATION ABSORBER

Governing Equations

Here, we consider propagation of transverse elastic waves (mainly asymmetric Lamb waves) in a metamaterial beam designed using the concept of vibration absorbers (Figure 1). The governing equations for a unit cell of an infinite metamaterial beam can be derived using the extended Hamilton principle $\int_0^L (\delta T - \delta\Pi + \delta W_{nc})\mathbf{d}t = 0$, where T is the kinetic energy, π is the elastic energy, and W_{nc} is the non-conservative work due to external loads. More than what is shown in Figure 1, we consider both translational and rotational vibration absorbers in the free-body diagram of the unit cell model shown in Figure 3(a). It follows from Figure 3(a) that:

$$
\begin{aligned}
\delta T &= -\int_{-L/2}^{L/2} (\rho A\ddot{w}\delta w + \rho I\ddot{w}'\delta w')\mathrm{d}x - m\ddot{v}\delta v \\
&\quad - J\ddot{\phi}\delta\phi - \hat{m}\ddot{w}_0\delta w_0 \\
&= \int_{-L/2}^{L/2} (-\rho A\ddot{w} + \rho I\ddot{w}'')\delta w\,\mathrm{d}x - m\ddot{v}\delta v - J\ddot{\phi}\delta\phi \\
&\quad - \hat{m}\ddot{w}_0\delta w_0 - \rho I\ddot{w}'_1\delta w_1 + \rho I\ddot{w}'_{-1}\delta w_{-1}
\end{aligned}
$$

$$
\begin{aligned}
\delta\Pi &= \int_{-L/2}^{L/2} EIw''\delta w''\,\mathrm{d}x + k(v - w_0)(\delta v - \delta w_0) \\
&\quad + \tau(\phi - \theta_0)(\delta\phi - \delta\theta_0) \\
&= \int_{-L/2}^{L/2} EIw^{iv}\delta w\,\mathrm{d}x + k(v - w_0)(\delta v - \delta w_0) \\
&\quad + \tau(\phi - \theta_0)(\delta\phi - \delta\theta_0) \\
&\quad + EI(w''_1\delta\theta_1 - w''_{0+}\delta\theta_0 + w''_{0-}\delta\theta_0 - w''_{-1}\delta\theta_{-1} \\
&\quad - w'''_1\delta w_1 + w'''_{0+}\delta w_0 - w'''_{0-}\delta w_0 + w'''_{-1}\delta w_{-1}) \\
\delta W_{nc} &= EIw''_1\delta\theta_1 + (\rho I\ddot{w}'_1 - EIw'''_1)\delta w_1 - EIw''_{-1}\delta\theta_{-1} \\
&\quad + (EIw'''_{-1} - \rho I\ddot{w}'_{-1})\delta w_{-1} \\
\Rightarrow 0 &= \int_{-L/2}^{L/2} (\rho A\ddot{w} - \rho I\ddot{w}'' + EIw^{iv})\delta w\,\mathrm{d}x \\
&\quad + EI(w'''_{0+}\delta w_0 - w'''_{0-}\delta w_0 - w''_{0+}\delta\theta_0 + w''_{0-}\delta\theta_0) \\
&\quad + k(v - w_0)(\delta v - \delta w_0) + \tau(\phi - \theta_0)(\delta\phi - \delta\theta_0) \\
&\quad + m\ddot{v}\delta v + J\ddot{\phi}\delta\phi + \hat{m}\ddot{w}_0\delta w_0 \\
&= \int_{-L/2}^{L/2} \big(\rho A\ddot{w} - \rho I\ddot{w}'' + EIw^{iv} + [EI(w'''_{0+} - w'''_{0-}) \\
&\quad + k(w_0 - v) + \hat{m}\ddot{w}_0]\delta(x)\big)\delta w\,\mathrm{d}x \\
&\quad + [EI(-w''_{0+} + w''_{0-}) - \tau(\phi - \theta_0)]\delta\theta_0 \\
&\quad + [m\ddot{v} + k(v - w_0)]\delta v + [J\ddot{\phi} + \tau(\phi - \theta_0)]\delta\phi,
\end{aligned}
\tag{3}
$$

where A, I, E, and ρ are the beam's cross-sectional area, area moment, Young's modulus, and mass density, respectively. Moreover, L is the cell length; $\hat{m}, J$, and τ are the mass, rotary inertia, and torsional spring

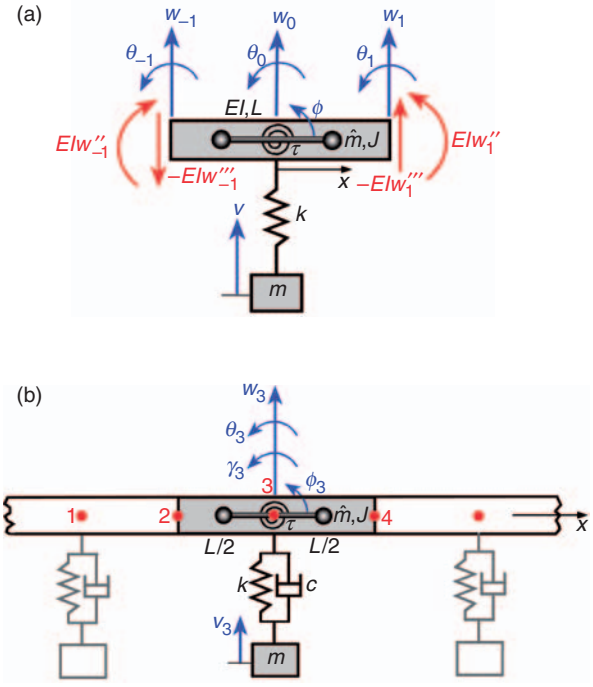

Figure 3. *Modeling of an infinite metamaterial beam: (a) free-body diagram of a unit cell, and (b) finite element modeling.*

constant of the rotational absorber; m and k are the mass and spring constant of the translational absorber; $\delta(x)$ is the Dirac delta function; $w' \equiv \partial w/\partial x \equiv \theta$; $\dot{w} \equiv \partial w/\partial t$, and $\theta_0 \equiv w'(0,t)$. Furthermore, $EIw''_{0^-} \neq EIw''_{0^+}$ and $EIw'''_{0^-} \neq EIw'''_{0^+}$ because the vibration absorbers create a concentrated bending moment and a concentrated shear force at $x=0$. Setting the coefficients of δw, δv, $\delta\phi$, and $\delta\theta_0$ in Equation (3) to zero yields the following governing equations:

$$\rho A\ddot{w} - \rho I\ddot{w}'' + EIw^{iv} + \left[EI\left(w'''_{0^+} - w'''_{0^-}\right) + k(w_0 - v) + \hat{m}\ddot{w}_0\right]\delta(x) = 0 \quad (4a)$$

$$m\ddot{v} + k(v - w_0) = 0 \quad (4b)$$

$$J\ddot{\phi} + \tau(\phi - \theta_0) = 0 \quad (4c)$$

$$EI\left(w''_{0^-} - w''_{0^+}\right) = \tau(\phi - \theta_0) \quad (4d)$$

Homogenized Material Properties and Dispersion Equation

Dynamic characteristics of an infinite periodic structure can be derived by considering only a representative cell and making use of the Bloch–Floquet theory (Brillouin, 1953). Accordingly, an elastic wave propagating through the unit cell shown in Figure 3(a) can be assumed to have:

$$w(x,t) = qe^{j(\beta x - \Omega t)}, \quad v(t) = pe^{-j\Omega t}, \quad \phi(t) = \varphi e^{-j\Omega t}, \quad (5)$$

where β, $\lambda(=2\pi/\beta)$, and Ω are the wave number, wavelength, and vibration frequency, respectively. The phase velocity of an elastic wave is $c_p = \lambda\Omega/(2\pi) = \Omega/\beta$. The modal vibration frequency of a standing wave is often represented by ω in structural dynamics, and the corresponding wave has a zero group velocity (i.e., $c_g = d\Omega/d\beta = 0$). Hence, we use Ω to represent the vibration frequency of an elastic wave having an arbitrary wavelength because it often corresponds to a traveling wave caused by an external excitation at a frequency Ω. If the beam is to be treated as a homogenized uniform beam, one can integrate Equation (4a) over the cell length L and use Equation (5) to obtain:

$$\int_{-L/2}^{L/2} \rho(A\ddot{w} - I\ddot{w}'')dx + EIw'''_1 - EIw'''_{-1} + k(w_0 - v) + \hat{m}\ddot{w}_0 = 0 \Leftrightarrow \bar{m}\ddot{w}_0 + \bar{k}w_0 + k(w_0 - v) = 0$$
$$\bar{m} \equiv \frac{2\rho(A + I\beta^2)\sin(\beta L/2)}{\beta} + \hat{m}, \quad \bar{k} \equiv 2EI\beta^3\sin(\beta L/2), \quad (6a)$$

which indicates that the beam segment is treated as a lumped mass $\bar{m}$ and a massless spring $\bar{k}$. However, $\bar{m}$ and $\bar{k}$ changes with the wave number β. Substituting Equation (5) into Equations (4b), (4c), and (6a) and setting the determinant of the coefficients of the three algebraic equations containing unknowns p, q, and φ to zero yields the following dispersion equation:

$$\left[\Omega^4 - \left(\bar{\Omega}^2 + \frac{k}{\bar{m}} + \frac{\bar{k}}{\bar{m}}\right)\Omega^2 + \bar{\Omega}^2\frac{\bar{k}}{\bar{m}}\right]\left(\Omega^2 - \frac{\tau}{J}\right) = 0,$$
$$\bar{\Omega} \equiv \sqrt{\frac{k}{m}} = \sqrt{\frac{\tau}{J}} \quad (6b)$$

Note that the integration shown in Equation (6a) transforms the system consisting of a continuum and two discrete DOFs (i.e., Equations (4a)–(4c)) into a system of 3 DOFs. The discontinuity shown in Equation (4d) is not and cannot be accounted for because of the use of Equation (5).

The effective mass density $\tilde{\rho}$ and effective Young's modulus $\tilde{E}$ can be defined by using Equations (5) and (6a) and ignoring (i.e., not knowing the existence of) the vibration absorbers as:

$$\tilde{\rho} \equiv \frac{EIw'''_{-1} - EIw'''_1}{\int_{-L/2}^{L/2}(A\ddot{w} - I\ddot{w}'')dx} = \frac{EI\beta^4}{(A + I\beta^2)\Omega^2},$$
$$\tilde{E} \equiv \frac{\int_{-L/2}^{L/2}\rho(A\ddot{w} - I\ddot{w}'')dx}{Iw'''_{-1} - Iw'''_1} = \frac{\rho(A + I\beta^2)\Omega^2}{I\beta^4} \quad (7)$$

If $\beta = j\alpha$ and $\alpha > 0$, $w(x,t) = qe^{-\alpha x}e^{-j\Omega t}$ indicates an evanescent (non-propagating) wave and a stopband exists. However, $\tilde{\rho}$ and $\tilde{E}$ are negative only if α is big enough to make $A + I\beta^2 = A - I\alpha^2 < 0$. Hence, it is inappropriate to use the sign of $\tilde{\rho}$ or $\tilde{E}$ to determine the existence of stopbands for metamaterial beams. For longitudinal elastic waves in a bar, a negative effective mass density indicates the existence of a stopband (Huang et al., 2009; Pai, 2010). Instead of creating negative effective mass density or Young's modulus and hence stopbands, the actual working mechanism of metamaterial beams is how conventional vibration absorbers work against external loads, as shown next.

Actual Working Mechanism

In Figure 3(a), if the internal shear force on the beam at $x = 0^-$ is $V_{0^-}(t) = -EIw'''(0^-,t) = F_0\cos\Omega t$ and $w_0 = a_0\cos\Omega t$, we obtain the steady-state solution $v = w_0\bar{\Omega}^2/(\bar{\Omega}^2 - \Omega^2)$ from Equation (4b), and hence, the internal shear force $V_{0^+}(t)$ on the beam at $x = 0^+$ should be:

$$V_{0^+}(t) \equiv -EIw'''(0^+,t) = -EIw'''(0^-,t) - k(v - w_0) + \hat{m}\ddot{w}_0 = \left(F_0 - \left\{\frac{k}{\bar{\Omega}^2 - \Omega^2} + \hat{m}\right\}\Omega^2 a_0\right)\cos\Omega t \quad (8)$$

Equation (8) shows that the absorber reduces the force amplitude from F_0 to $F_0 - [k/(\bar{\Omega}^2 - \Omega^2) + \hat{m}]\Omega^2 a_0$ when $\Omega > \bar{\Omega}$, $k/(\bar{\Omega}^2 - \Omega^2) + \hat{m} < 0$, and $F_0 a_0 < 0$ or when $\Omega < \bar{\Omega}$ and $F_0 a_0 > 0$, and this is the actual working mechanism of translational wave absorbers.

If the internal bending moment on the beam at $x = 0^-$ is $M_{0^-}(t) = EIw''(0^-, t) = B_0 \cos \Omega t$ and $\theta_0 = b_0 \cos \Omega t$, we obtain the steady-state solution $\phi = \theta_0 \bar{\Omega}^2/(\bar{\Omega}^2 - \Omega^2)$ from Equation (4c), and hence, the internal bending moment $M_{0^+}(t)$ on the beam at $x = 0^+$ should be:

$$M_{0^+}(t) \equiv EIw''(0^+, t) = EIw''(0^-, t) - \tau(\phi - \theta_0) = \left(B_0 + \frac{\tau \Omega^2 b_0}{\Omega^2 - \bar{\Omega}^2}\right) \cos \Omega t \tag{9}$$

Equation (9) shows that the absorber reduces the bending moment amplitude from B_0 to $B_0 + \tau\Omega^2 b_0/(\Omega^2 - \bar{\Omega}^2)$ when $\Omega > \bar{\Omega}$ and $B_0 b_0 < 0$ or when $\Omega < \bar{\Omega}$ and $B_0 b_0 > 0$, and this is the actual working mechanism of rotational wave absorbers.

Finite Element Modeling

The continuity assumed for w in Equation (5) and the averaging shown in Equation (6a) cannot account for the discontinuity $EIw''_{0^-} \neq EIw''_{0^+}$ in Equation (4d). Hence, the influence of the torsional absorber cannot be averaged into the dispersion Equation (6b), which makes $\Omega = \sqrt{\tau/J}$ a separate answer. In other words, this averaging approach is not really appropriate for such a highly inhomogeneous built-up material. Such homogenized models can be used only for waves having $\lambda \gg L$ such that the wave profile between two adjacent absorbers can be approximated by a smooth function like the one shown in Equation (5). For metamaterial beams having far separated discrete absorbers or transverse waves of short wavelength, these models are invalid because they do not account for the discontinuities of w'' and w''' at $x = 0$. On the other hand, displacement-based finite element modeling can easily account for such discontinuities and will be used for later detailed simulations, as shown next.

As shown in Figure 3(b), we discretize the beam segment of each cell into two beam elements. Because shear deformation and rotary inertias are significantly influential on propagation of elastic waves in beams (Graff, 1975), we adopt Timoshenko's beam theory and include rotary inertias in the finite element modeling. Accordingly, the variations of kinetic and elastic energies in Equation (3) are modified as:

$$\begin{aligned}\delta T = &- \int_{-L/2}^{L/2} [\rho A \ddot{w} \delta w + \rho I(\ddot{w}' - \ddot{\gamma})(\delta w' - \delta\gamma)] \mathrm{d}x \\ &- m\ddot{v}\delta v - J\ddot{\phi}\delta\phi - \hat{m}\ddot{w}_0 \delta w_0 \\ \delta \Pi = &\int_{-L/2}^{L/2} [EI(w'' - \gamma')\delta(w'' - \gamma') + k_s GA\gamma\delta\gamma] \mathrm{d}x \\ &+ k(v - w_0)(\delta v - \delta w_0) + \tau(\phi - \theta_0 + \gamma_0) \\ &\times (\delta\phi - \delta\theta_0 + \delta\gamma_0),\end{aligned} \tag{10a}$$

where G is the shear modulus, γ is the shear rotation angle, w' is the total rotation, and $w' - \gamma$ is the bending rotation. Because only uniform isotropic beams with rectangular cross sections will be considered, the shear correction factor k_s is set to be 5/6 (Pai, 2007). The weak form shown in Equation (10a) can be discretized by using linear shape functions for ϕ and γ, and Hermite cubic polynomials for w. Hence, there are 3 DOF w, w', and γ at each of the four nodes in Figure 3(b), and 2 DOF v and ϕ for the translational and rotational absorbers at nodes 1 and 3. To determine dynamic characteristics of a periodic structure having an infinite length (i.e., without influences of boundary conditions), only the four nodes marked in Figure 3(b) need to be modeled according to the Bloch–Floquet theory (Brillouin, 1953). Hence, there are 16 DOFs in total in the following governing equations from conventional finite element modeling using the extended Hamilton principle:

$$\begin{aligned}[M]\{\ddot{q}\} + [K]\{q\} = \{0\}, \{q\} \\ = \{w_1, \theta_1, \gamma_1, \ldots, w_4, \theta_4, \gamma_4, v_1, v_3, \phi_1, \phi_3\}^T,\end{aligned} \tag{10b}$$

where the dampers shown in Figure 3(b) are not considered here. According to the Bloch–Floquet theory, we have:

$$\begin{aligned}\{w_1, \theta_1, \gamma_1, v_1, \phi_1\} = \{w_3, \theta_3, \gamma_3, v_3, \phi_3\} e^{-j\beta L}, \\ \{w_4, \theta_4, \gamma_4\} = \{w_2, \theta_2, \gamma_2\} e^{j\beta L}\end{aligned} \tag{11}$$

Substituting Equation (11) into Equation (10b) reduces the mass and stiffness matrices into 8×8 matrices $[\hat{M}]$ and $[\hat{K}]$. For each wave number β, $\left|[\hat{K}] - \Omega^2[\hat{M}]\right| = 0$ yields eight values for Ω^2. However, it follows from Equation (5) that a complex value for Ω indicates a mode that either decays or diverges exponentially and does not need to be considered. The main interest is on the ones close to the absorber's resonant frequency $\bar{\Omega} \equiv \sqrt{k/m} = \sqrt{\tau/J}$.

NUMERICAL RESULTS

To show the actual working mechanism of broadband vibration absorbers and how to design them, we consider infinite and finite metamaterial beams with different distributions of absorbers.

Infinite Beams with Uniform Absorbers

First, we consider an infinite metamaterial beam (Figures 1 and 3(a)) having:

$$\begin{aligned} &L = 10\,\text{mm},\ b = 5\,\text{mm},\ h = 3\,\text{mm},\ A = bh,\\ &E = 72.4\,\text{GPa},\ \nu = 0.33,\ \rho = 2780\,\text{kg/m}^3\\ &m = 0.1\rho AL,\ k = m\bar{\Omega}^2,\ \hat{m} = 0.1\rho AL,\\ &J = \hat{m}L^2/4, \tau = J\bar{\Omega}^2,\ \bar{\Omega} \equiv 2400\,\text{Hz}, \end{aligned} \tag{12}$$

where $\text{Hz} = 2\pi$ rad/s. Figure 4(a) shows the dispersion curves obtained from Equations (10b) and (11) with $m/(\rho AL) = 0.1, 0.3, 0.5$ and $\hat{m}/(\rho AL) = 0.1$. The dashed lines are obtained from Equation (6b) with $m/(\rho AL) = \hat{m}/(\rho AL) = 0.1$. Results from Equation (10b) account for the discontinuity $EIw''_{0-} \neq EIw''_{0+}$ and shear flexibility, but those from Equation (6b) do not. Shear flexibility actually does not cause significant differences for this case here because it is a thin beam. Because the $[\hat{M}]$ and $[\hat{K}]$ from Equation (10b) are 2π periodic and remain the same if $\exp(\pm j\beta L)$ is replaced with $\exp(\mp j\beta L)$, only $0 < \beta L \leq \pi$ needs to be examined in order to obtain all frequencies. Figure 4(a) shows that the stopband increases with the translational absorber's mass m. On the other hand, Figure 4(b) shows that the stopband decreases when the rotational absorber's mass $\hat{m}$ increases. For a rotational absorber with a small mass, it does not significantly interact with the beam, and hence, $\Omega = \sqrt{\tau/J}$ is a separate solution of Equation (6b), which represents the vertical line $\Omega/\bar{\Omega} = 1$ in Figure 4(a) and (b). When $\hat{m}$ increases, the rotational absorber interacts more with the beam through bending and shear rotations, curves the vertical line $\Omega = \sqrt{\tau/J}$ in Figure 4(b), and intends to increase the stopband by lowering the low-frequency bound, but the high-frequency bound is also reduced. Numerical simulations of finite beams with different boundary conditions also confirm this phenomenon. Moreover, because it is difficult to manufacture and integrate rotational absorbers with a beam in actual applications, rotational absorbers will not be considered hereafter.

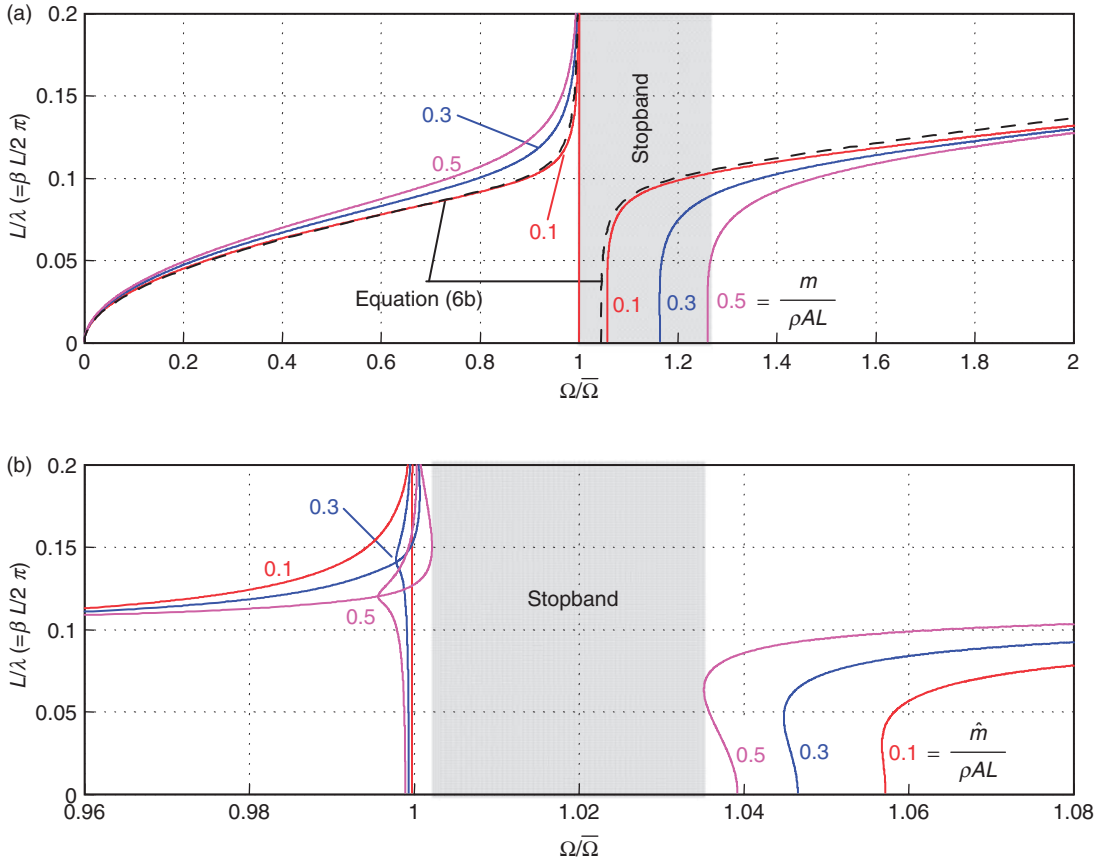

Figure 4. *Dispersion curves with $\bar{\Omega} = \sqrt{k/m} = \sqrt{\tau/J} = 2400$ Hz: (a) $m/(\rho AL) = 0.1, 0.3, 0.5$ with $\hat{m}/(\rho AL) = 0.1$, and (b) $\hat{m}/(\rho AL) = 0.1, 0.3, 0.5$ with $m/(\rho AL) = 0.1$.*

Note that a vertical line tangent to the dispersion curves in Figure 4(a) and (b) indicates a natural frequency of a standing vibration mode because the corresponding group velocity $c_g \equiv d\Omega/d\beta = 0$ (Graff, 1975). On the other hand, $d\Omega/d\beta \neq 0$ corresponds to a traveling wave. The most important phenomenon revealed by Figure 4(a) is that an elastic wave with a long wavelength (i.e., a low L/λ) can propagate at two different frequencies (or speeds), and this results in the existence of a stopband. The low-frequency motion is in an acoustic mode, and the high-frequency motion is in an optical mode, as shown later.

Finite Beams with Uniform Absorbers

Next, we consider a simply supported metamaterial beam consisting of 100 cells (Figure 3(b)) and:

$$\begin{aligned}
&\tilde{L} = 100\,\text{cm},\ L = \tilde{L}/100,\ b = 5\,\text{mm},\ h = 3\,\text{mm},\\
&A = bh,\ E = 72.4\,\text{GPa},\ \nu = 0.33,\ \rho = 2780\,\text{kg/m}^3\\
&m = 0.1\rho AL,\ k = m\bar{\Omega}^2,\ c = 2\varsigma\sqrt{mk},\ \varsigma = 0.01,\\
&\bar{\Omega} \equiv 2400\,\text{Hz},\ \hat{m} = J = 0\\
&F_0 = \rho AL\bar{\Omega}\ \text{at}\ x = 5\,\text{mm},
\end{aligned} \tag{13}$$

where $\tilde{L}$ denotes the beam length, L is the cell length, and F_0 is the amplitude of a harmonic excitation force. Here, $F_0 = \rho AL\bar{\Omega}$ is chosen in order to have about the same order of vibration amplitudes for both low- and high-frequency vibrations. The beam is divided into 200 finite beam elements. Without absorbers, the first five natural frequencies are 6.94, 27.77, 62.47, 111.05, and 173.49 Hz. (The shear flexibility slightly reduces the third, fourth, and fifth frequencies from 62.48, 111.07, and 173.54 Hz, but significant changes happen to higher modes.) The mode shapes are essentially $a_i \sin(i\pi x/\tilde{L})$ for the i-th mode. Adding the absorbers with massless rigid springs increases the total mass of the beam by 20% and decreases the first five frequencies to 6.34, 25.35, 57.02, 101.36, and 158.33 Hz. Here, we add a discrete damper to each absorber, as shown in Figure 3(b). The corresponding finite element model and FRF matrix $[H]$ are:

$$\begin{aligned}
&[M]\{\ddot{q}\} + [C]\{\dot{q}\} + [K]\{q\} = \{F\},\\
&\{F\} = \{0, 0, 0, F_0 e^{j\Omega t}, 0, \ldots\}^T\\
&[H] = [-\Omega^2[M] + j\Omega[C] + [K]]^{-1},\\
&\{q\} = [H]\{F\} = \{H_{i4}\}F_0 e^{j\Omega t}
\end{aligned} \tag{14}$$

Figure 5(a) shows the FRF $H_{101,2}$ of the transverse displacement of node 101 at $x = \tilde{L}/2$ with a harmonic excitation at node 2 at $x = \tilde{L}/200$. Setting $k \to \infty$ is equivalent to adding the translational absorbers as dead masses to the beam, and hence, the absorbers do not function at all. The FRF with $\varsigma = 0.0001$ reveals that the absorbers designed with $\sqrt{k/m} = \bar{\Omega} = 2400\,\text{Hz}$ create a stopband above $\bar{\Omega}$, as predicted by Equations (6b) and (10b) and shown in Figure 4(a). However, many small peaks beside the stopband exist, and they are caused by local modal vibrations of the absorbers. Fortunately, if the damping ratio of each absorber is slightly increased to $\varsigma = 0.01$, those peaks are dramatically reduced. Hence, damping is needed for such vibration absorbers. If the absorbers are designed with $\sqrt{k/m} = \bar{\Omega} = 1000\,\text{Hz}$, Figure 5(b) shows again that the absorbers create a stopband above $\bar{\Omega}$, and the many small peaks beside the stopband can be suppressed by increasing the damping ratio.

Figure 6(a)–(c) shows the maximum steady-state wave profiles when $\sqrt{k/m} = \bar{\Omega}/r$, $\varsigma = 0.01$, $\Omega = \bar{\Omega} = 2400\,\text{Hz}$, and $r = 0.8, 1.02, 1.3$. Figure 4(a) shows that the stopband exists within $1 \leq \Omega/\bar{\Omega} < 1.057$. Figure 6(b) shows that, if the incoming wave's frequency Ω is within the absorbers' stopband, the first few absorbers work against and suppress the incoming wave. Figure 6(a) and (c) shows that $\Omega < \bar{\Omega}/r = \sqrt{k/m}$ corresponds to an acoustic mode (i.e., w and v are in phase) with a short wavelength, and $\Omega > \bar{\Omega}/r = \sqrt{k/m}$ corresponds to an optical mode (i.e., w and v are out of phase) with a long wavelength. The slight decay of amplitude in Figure 6(a) and (c) are caused by damping.

Figure 6(a)–(c) reveals that propagation of transverse waves in a metamaterial beam is similar to that of longitudinal waves in a metamaterial bar (Pai, 2010). Because the proposed metamaterial beam uses resonant inertia forces of absorbers to create stopbands, it requires less additive masses and is more efficient than conventional band-gap grid structures that create stopbands by adding only lumped masses at nodes (Diaz et al., 2005). However, the proposed absorber subsystems need to have dampers in order to reduce those small frequency response peaks beside the stopband (Figure 5), and hence, the cost is expected to be higher.

Finite Beams with Linearly Varying Absorbers

Figure 6(b) shows that only the first few absorbers work against and suppress the incoming wave, and Figure 5(a) and (b) shows that each absorber can only absorb waves within a small frequency band that the absorber is designed for. Hence, a metamaterial beam with distributed absorbers designed for different frequency bands should be able to absorb broadband waves. Without adding extra masses, Figure 7(a) shows that the frequency range of low-amplitude response is significantly increased by redistributing the springs of absorbers to have:

$$\begin{aligned}
&m = 0.1\rho AL,\ k = m(\bar{\Omega}/r)^2,\ c = 2\varsigma\sqrt{mk},\ \varsigma = 0.01,\\
&\bar{\Omega} = 2400\,\text{Hz}\\
&r = 1.5 - 0.005(i-1),\ i = 2, 4, \ldots, 200
\end{aligned} \tag{15}$$

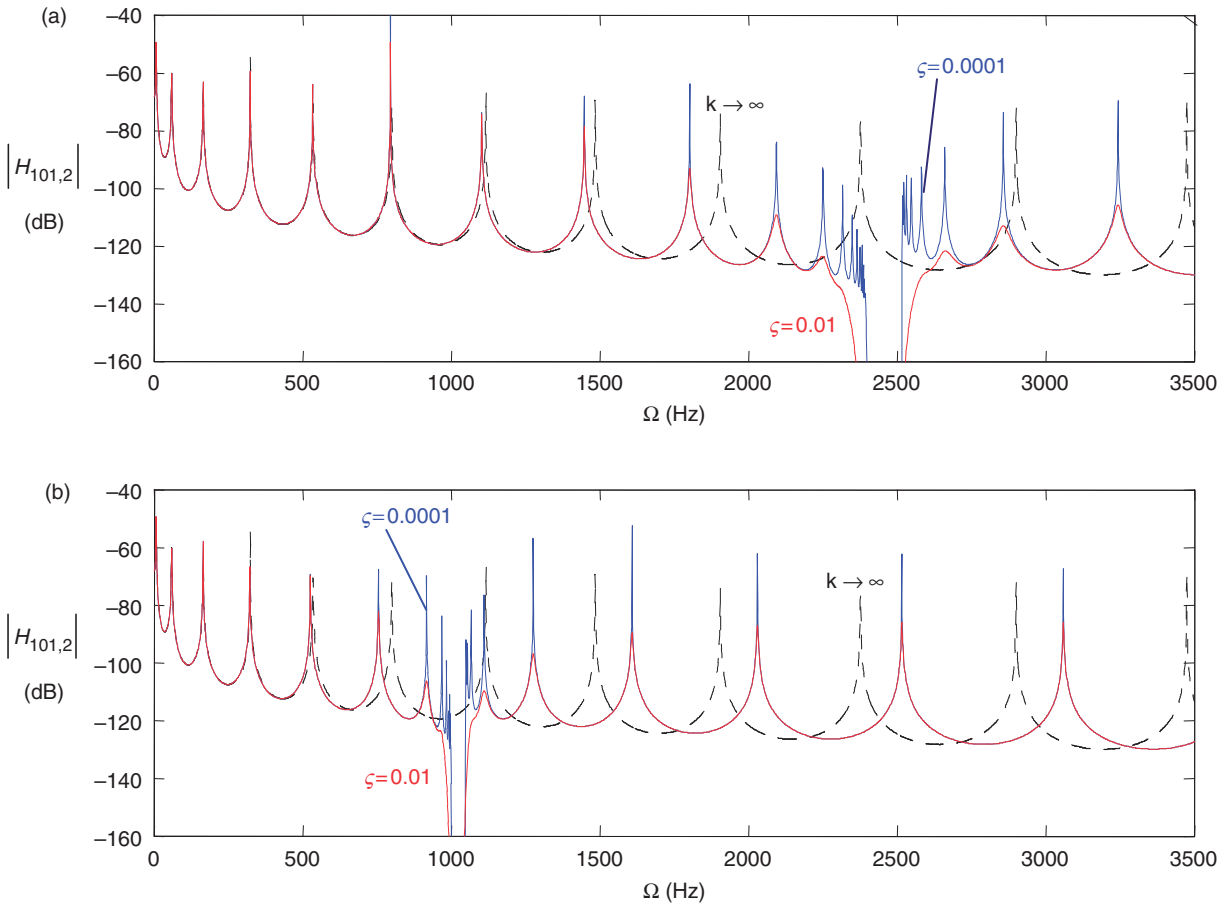

Figure 5. *Frequency response functions $H_{101,2}$ with $m = 0.1\rho AL$ and $\hat{m} = 0$: (a)$\sqrt{k/m} = \bar{\Omega} = 2400$ Hz, and (b)$\sqrt{k/m} = \bar{\Omega} = 1000$ Hz, where $k \to \infty$(dashed line), $\varsigma = 0.0001$(blue line), or $\varsigma = 0.01$(red line).*

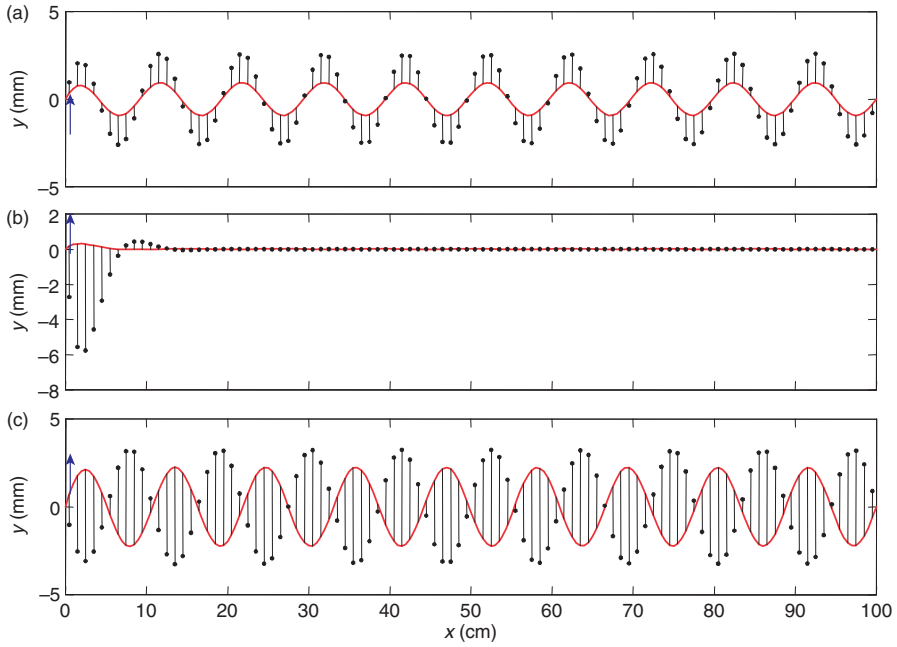

Figure 6. *Steady-state wave profiles when $\Omega = \bar{\Omega} = 2400$ Hz: (a) $r = 0.8$, (b) $r = 1.02$, and (c) $r = 1.3$.*

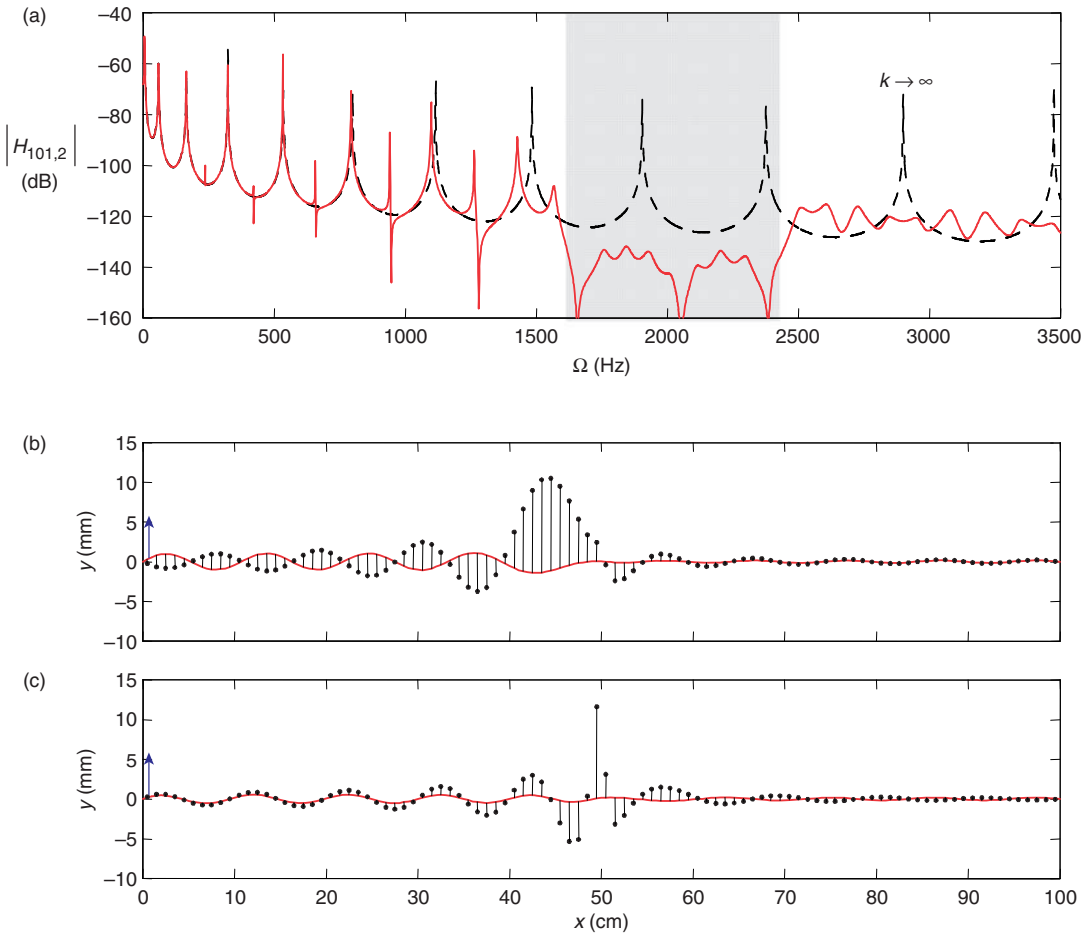

Figure 7. *A simply supported metamaterial beam with $\sqrt{k/m} = \bar{\Omega}/r$ and $\bar{\Omega} = 2400$ Hz: (a) FRF with $r = 1.5 - 0.005(i-1)$, $i = 2, 4, \ldots, 200$, (b) steady-state wave profiles with $\Omega = \bar{\Omega}$ and $r = 1.5 - 0.005(i-1)$, $i = 2, 4, \ldots, 200$, and (c) steady-state wave profile with $\Omega = \bar{\Omega}$ and $r = 0.5 + 0.005(i-1)$, $i = 2, 4, \ldots, 200$.*

The spikes at $\Omega = 1264$, 942, 658 Hz, and so on are caused by local resonance of absorbers. Figure 7(b) shows that the design takes advantage of the stopband effect to make absorbers move in their optical modes to create opposite inertia forces to absorb the incoming wave. On the other hand, Figure 7(c) shows that using the absorbers' acoustic mode for absorption is not efficient, and it highly depends on the few absorbers around $x = \tilde{L}/2$ to absorb the wave by vibrating at large amplitudes. Hence, it is better to locate absorbers designed with resonant frequencies lower than that of the incoming wave to meet with the wave first if the direction of the incoming wave is known. If the direction is unknown (see, e.g., Figure 1), it is better to design absorbers into subgroups distributed along the beam and the resonant frequencies of absorbers of each subgroup cover a wide range of frequency band.

Finite Beams with a Few Absorbers

To reveal the actual working mechanism of the metamaterial beam shown in Figures 1 and 3(b), we consider a beam with five absorbers at $x = 48.5$, 49.5, 50.5, 51.5, 52.5 cm. Figure 8(a) shows that a vibration absorber with a local resonant frequency higher than the incoming wave's frequency cannot create a significant inertia force to balance out the internal shear force because the beam and absorber move in phase. On the other hand, Figure 8(b) and (c) shows that a vibration absorber with a local resonant frequency lower than the incoming wave's frequency creates a significant inertia force to balance out the internal shear force because the beam and absorber move in an optical mode (i.e., out of phase) that results in the stopband effect, just like Equation (8) predicts. In Figure 8(c), the internal shear force is calculated using $-EI(w''' - \gamma'') + \rho I(\ddot{w}' - \ddot{\gamma})$ in order to clearly show its discontinuity. Note that the five absorbers in Figure 8(b) only add 2.5% weight to the whole structure and it works well. In the literature, the stopband effect is often explained by using the dynamical effective material properties averaged over a unit cell, and the main idea for designing a broadband absorber is to increase the stopband. On the other hand, Figure 8(c) shows that the stopband effect is actually caused by resonance-induced inertia forces. Hence, the

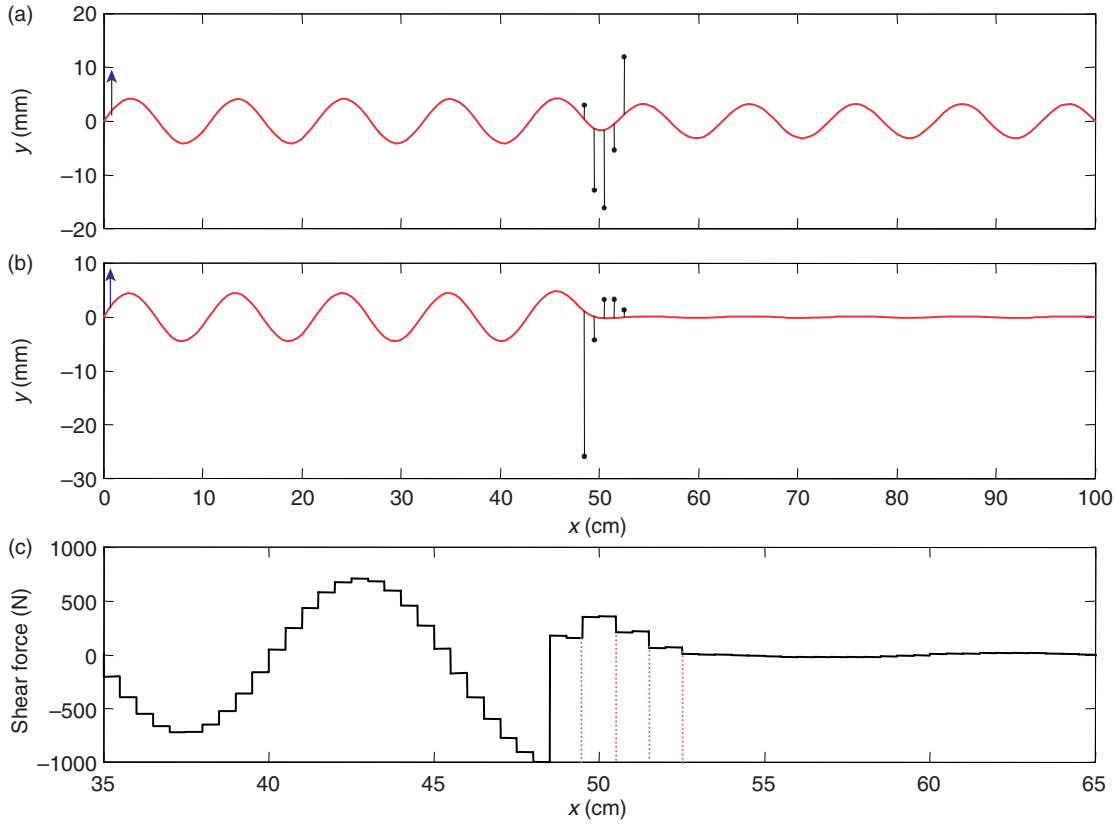

Figure 8. *A metamaterial beam with five absorbers having $m = 0.5\rho AL$, $\sqrt{k/m} = \bar{\Omega}/r$, and $\Omega = \bar{\Omega} = 2400$ Hz: (a) steady-state wave profile with $r = 0.95$, (b) steady-state wave profile with $r = 1.02$, and (c) distribution of internal shear force with $r = 1.02$.*

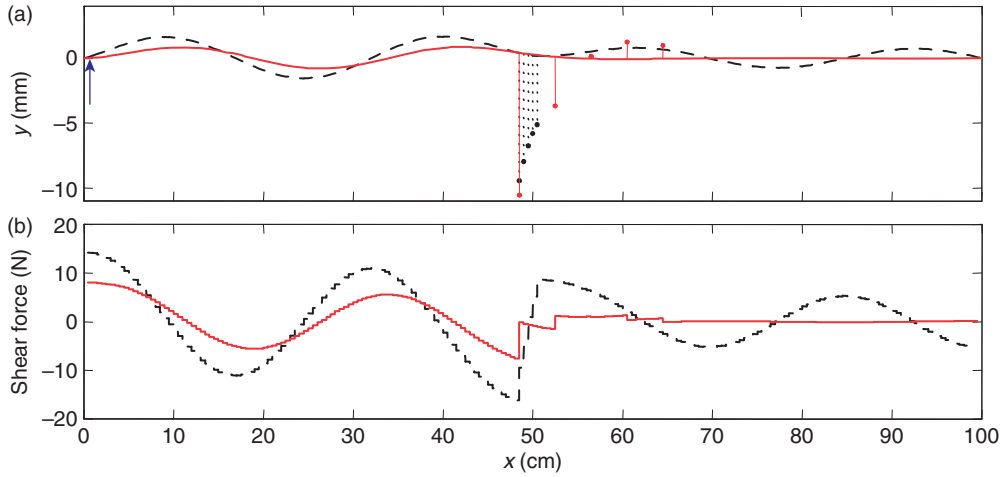

Figure 9. *A metamaterial beam with five absorbers having $m = 0.5\rho AL$, $\sqrt{k/m} = \bar{\Omega}/r$, $\Omega = \bar{\Omega} = 300$ Hz, and $r = 1.02$: (a) steady-state wave profiles, and (b) internal shear forces.*

correct way to increase the range of a stopband is to use small mechanical vibration absorbers with resonance frequencies covering a wide and continuous range of frequencies.

For a high-frequency wave, because boundary conditions do not have significant influences on its propagation, the locations of and distance between absorbers do not have significant influences on its absorption of waves, as shown in Figure 8(b). Because some of the five absorbers are displaced to the upper side and some to the lower sides, the absorbers undergo local resonance among themselves to create shear forces and bending moments to straighten the beam, and hence, its absorption of waves is not significantly affected by

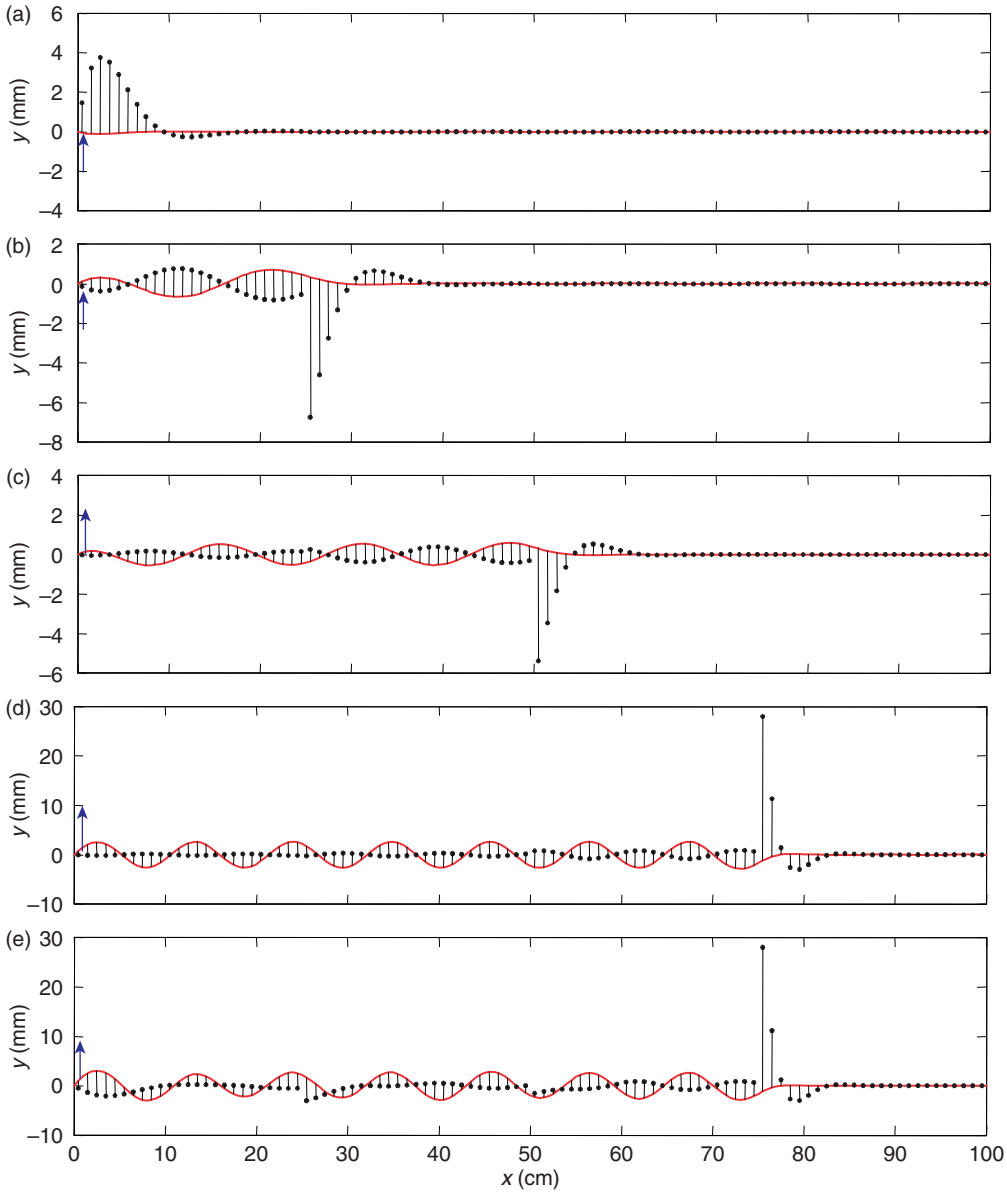

Figure 10. *Steady-state wave profiles of a simply supported metamaterial beam with* $\sqrt{k/m}=\bar{\Omega}/r, \bar{\Omega}=2400\text{Hz}$, $r=4.08(i=2,4,\ldots,50)$, $3.06(i=52,\ldots,100), 2.04(i=102,\ldots,150), 1.02(i=152,\ldots,200)$: *(a)* $F=\rho AL(\bar{\Omega}/4)\sin(\bar{\Omega}t/4)$, *(b)* $F=\rho AL(\bar{\Omega}/3)\sin(\bar{\Omega}t/3)$, *(c)* $F=\rho AL(\bar{\Omega}/2)\sin(\bar{\Omega}t/2)$, *(d)* $F=\rho AL\bar{\Omega}\sin(\bar{\Omega}t)$, *and (e)* $F=\sum_{s=1}^{4}\rho AL(\bar{\Omega}/s)\sin(\bar{\Omega}t/s)$.

boundary conditions. On the other hand, boundary conditions have significant influences on the propagation of a low-frequency wave, and hence, the locations of and distance between absorbers do have significant influences on its absorption of waves, as shown in Figure 9(a) and (b). Figure 9(a) shows that, if absorbers are close to each other, all absorbers are displaced to the same side of the beam. This indicates that the absorbers undergo global resonance with the beam, and they do not decrease the vibration amplitude but only change the phase of wave propagation, as shown in Figure 9(b). (If it is an infinite beam, Equations (6b) and (10b) predict that the absorbers can decrease the wave amplitude because $\Omega > \bar{\Omega}/r = \sqrt{k/m}$ and the wave's frequency is within the stopband of the absorbers.) If the absorbers are spread over $\lambda/2$, Figure 9(a) and (b) shows that the same five absorbers can suppress the vibration by global resonance. Hence, the absorption of low-frequency waves is significantly affected by boundary conditions and the closeness between the excitation frequency and the beam's natural frequencies. Moreover, low-frequency absorbers often undergo large-amplitude vibrations because the vibration frequency is low and the corresponding inertia forces $-m\ddot{v}$ $(=\Omega^2 mv)$ to work against the internal shear force need to be increased by having a large vibration

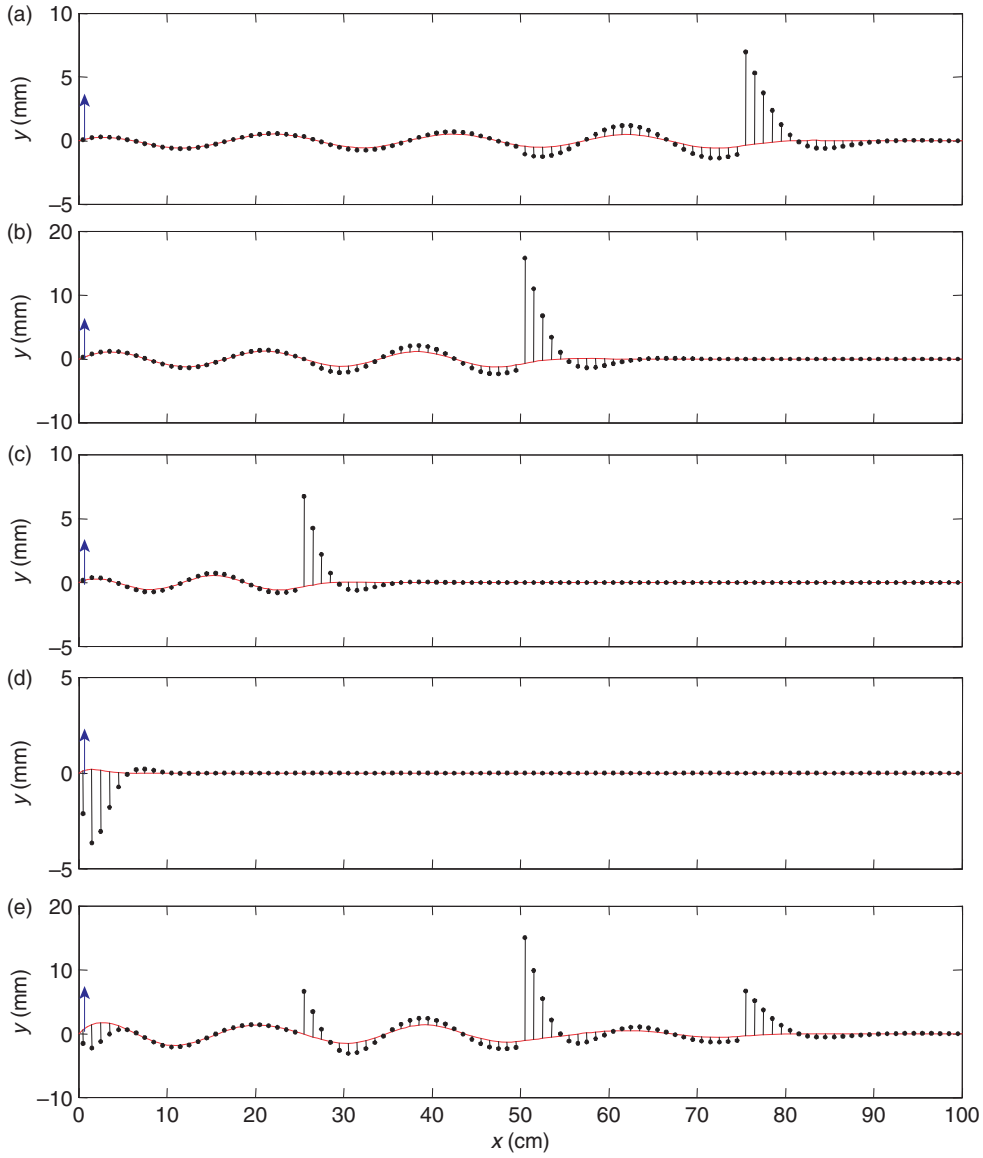

Figure 11. *Steady-state wave profiles of a simply supported metamaterial beam with* $\sqrt{k/m}=\bar{\Omega}/r, \bar{\Omega}=2400$*Hz,* $r=1.02(i=2,4,\ldots,50), 2.04(i=52,\ldots,100), 3.06(i=102,\ldots,150), 4.08(i=152,\ldots,200)$*: (a)* $F=\rho AL(\bar{\Omega}/4)\sin(\bar{\Omega}t/4)$*, (b)* $F=\rho AL(\bar{\Omega}/3)\sin(\bar{\Omega}t/3)$*, (c)* $F=\rho AL(\bar{\Omega}/2)\sin(\bar{\Omega}t/2)$*, (d)* $F=\rho AL\bar{\Omega}\sin(\bar{\Omega}t)$*, and (e)* $F=\sum_{s=1}^{4}\rho AL(\bar{\Omega}/s)\sin(\bar{\Omega}t/s)$*.*

amplitude. Hence, in the design of low-frequency absorbers for a structure, the structure's boundary conditions need to be considered, and more massive absorbers need to be used and widely separated.

Finite Beams with Absorbers Divided Into Subgroups

Figures 4(a), 5(a), 5(b), 6(b), 7(a), 8(c), 9(a), and 9(b) clearly demonstrate and reveal that the actual working mechanism of the proposed metamaterial beam-like vibration absorber is based on the concept of conventional mechanical vibration absorbers. It uses the incoming wave to resonate absorbers to work in their optical mode at frequencies close to but above their resonance frequencies to create shear forces and bending moments to straighten the beam and stop the wave propagation. This concept can be easily used to design a metamaterial beam for absorbing broadband elastic waves. For example, Figure 10 shows how a wave consisting of four harmonics can be absorbed by a beam with four sections of absorbers designed as:

$$
\begin{aligned}
&L=\tilde{L}/100,\ m=0.2\rho AL,\ k=m(\bar{\Omega}/r)^2,\ c=2\varsigma\sqrt{mk},\\
&\varsigma=0.01,\ \bar{\Omega}=2400\,\mathrm{Hz}\\
&r=4.08(i=2,4,\ldots,50),\ 3.06(i=52,\ldots,100),\\
&\quad 2.04(i=102,\ldots,150),\ 1.02(i=152,\ldots,200)\\
&F=\sum_{s=1}^{4}\rho AL(\bar{\Omega}/s)\sin(\bar{\Omega}t/s)
\end{aligned}
\tag{16}
$$

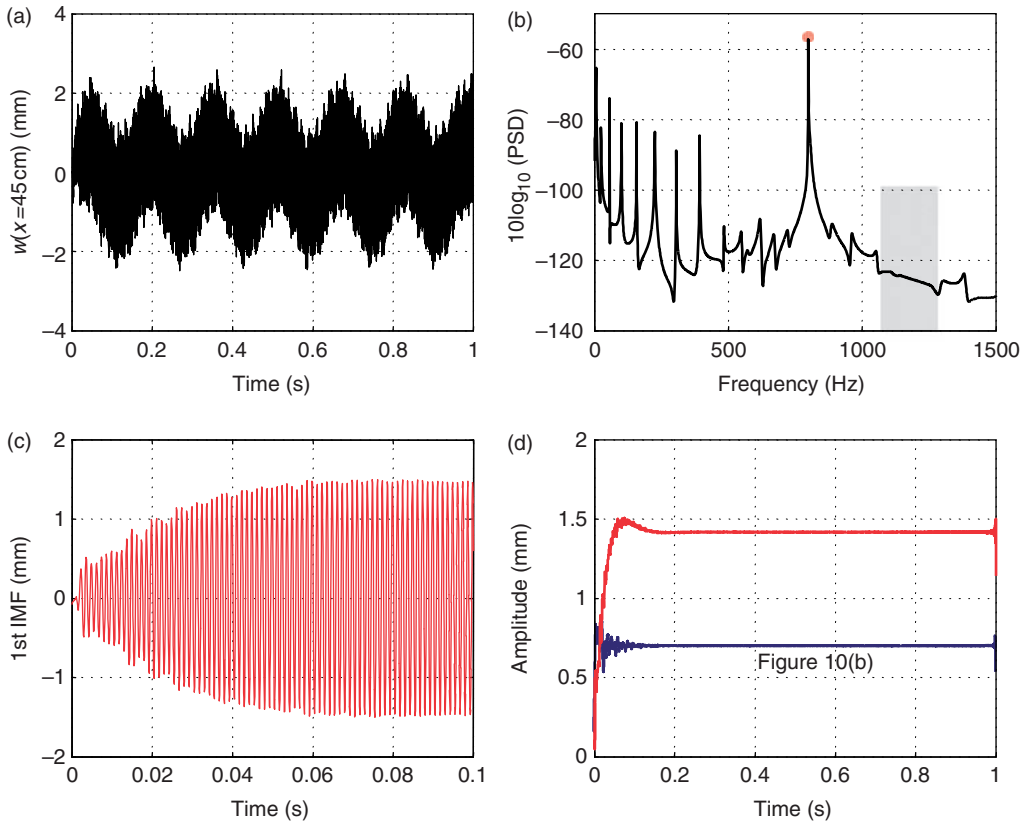

Figure 12. *Transient response of the metamaterial beam in Figure 11(b): (a) w(x = 45 cm, t), (b) PSD, (c) the first IMF of w(x = 45 cm, t), and (d) the time-varying amplitude of the first IMF, where the blue line is the amplitude of the first IMF of w(x = 20 cm,t) in Figure 10(b).*

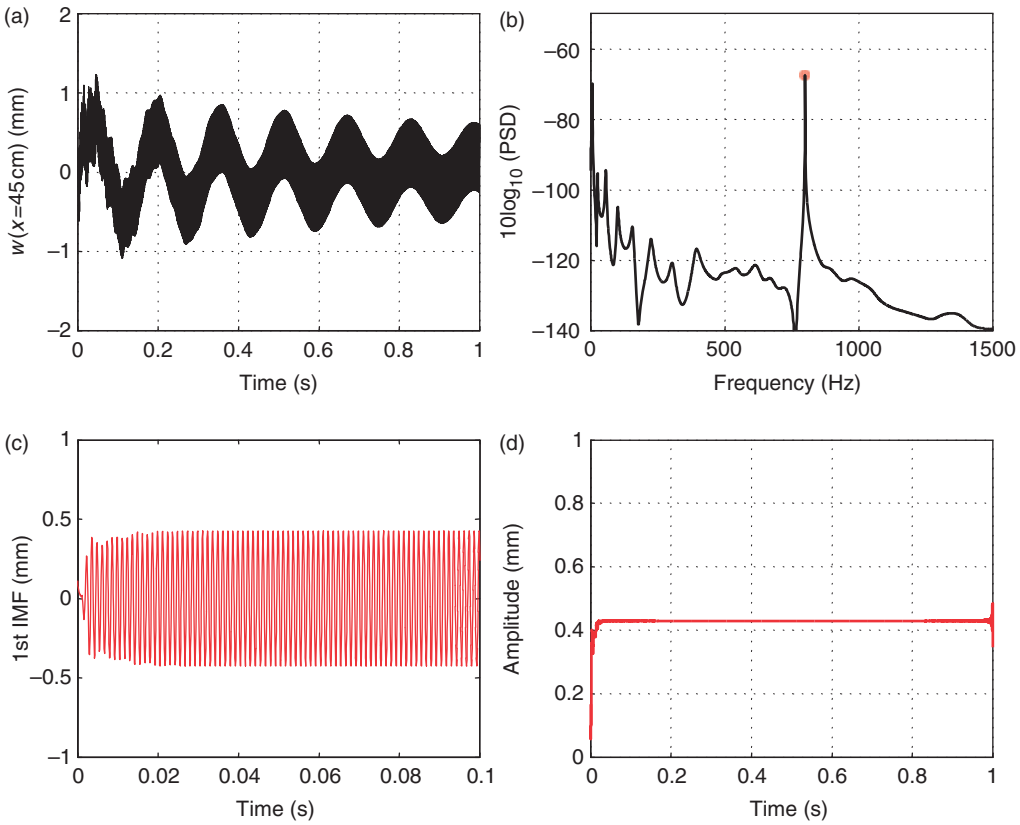

Figure 13. *Transient response of the metamaterial beam in Figure 11(b) with a modal damping of 0.03 for each mode: (a) w(x = 45 cm, t), (b) PSD, (c) the first IMF of w(x = 45 cm, t), and (d) the time-varying amplitude of the first IMF.*

Figure 10(a)–(d) shows that the wave excited by a single harmonic force $F = \rho AL(\bar{\Omega}/s)\sin(\bar{\Omega}t/s)$ is stopped at the beginning of the corresponding absorber section that is designed to stop it. When a high-frequency wave passes through an absorber section of soft springs, its amplitude decreases because it excites the absorbers to vibrate in their optical mode, especially those absorbers with resonance frequencies lower than but close to the wave's frequency. If the sequence of absorbers are reversed, Figure 11(a)–(d) shows that the wave excited by a single harmonic force $F = \rho AL(\bar{\Omega}/s)\sin(\bar{\Omega}t/s)$ is also stopped at the beginning of the corresponding absorber section that is designed to stop it, but the amplitudes are larger than those in Figure 10(a)–(c). When a low-frequency wave passes through an absorber section of hard springs, its amplitude almost remains the same because it excites the absorbers to vibrate in their acoustic modes, which do not have large relative motions between the beam and absorbers, and hence, the dampers do not dissipate energy significantly. Figures 10(e) and 11(e) reveal that different arrangements of absorber sections result in different vibration characteristics, but the arrangement shown in Figure 10 is recommended because of its damping characteristics.

The steady-state response shown in Figure 11(b) is due to a harmonic excitation at 800 Hz, and Figure 12(a) and (b) shows the corresponding transverse transient vibration of the beam at $x = 45$ cm during the first second and its power spectral density (PSD). Because the dampers of the second absorber section ($25\text{ cm} < x < 50\text{ cm}$) are designed to be effective around a resonance frequency 1200 Hz, Figure 12(b) shows that they are not effective for the forced response harmonic at 800 Hz, but they cause the groove around 1200 Hz. Because the dampers of the first, third, and fourth sections of absorbers are designed to be effective around resonance frequencies 2400, 800, and 600 Hz, respectively, the peaks below 500 Hz in Figure 12(b) indicate global resonance frequencies of the beam system and are essentially not suppressed by any damping at all because no material damping is assumed for the beam in this simulation. In Figure 12(a), the lowest frequency component is due to the free vibration of the first mode at 6.34 Hz, which is caused by the start-up effect and takes a very long time to die out because no material damping is assumed here and absorbers' discrete dampers are not designed for this frequency. The highest frequency component shown in Figure 12(c) and (d) is mainly the forced vibration at 800 Hz and is extracted as the first intrinsic mode function (IMF) by using the Hilbert–Huang transform (HHT) (Huang and Shen, 2005). It shows that this component reaches its steady state within less than 0.2 s because the dampers in the third section are designed to work around this frequency. On the other hand, the blue line in Figure 12(d) shows that the forced vibration component (at 800 Hz) of Figure 10(b) reaches its steady state at an even shorter time because the wave passes through the first section of absorbers and excite those absorbers to vibrate at their optical mode. Hence, those dampers in the first and second sections are effective for this wave.

If a modal damping ratio of 0.03 is assumed for each mode of the metamaterial beam shown in Figure 11(b), Figure 12(a)–(d) is changed into Figure 13(a)–(d). Figure 13(a) shows that high-frequency global modes excited by start-up decay quickly but low-frequency ones take a while to die out. Figure 13(b) shows that the added modal damping significantly reduces the resonance peaks of modes that are not directly excited. Figure 13(c) and (d) shows that the first IMF (i.e., the directly excited component) from HHT reaches its steady state very quickly and its amplitude is smaller than that in Figure 12(d).

These results and discussions reveal that it is important for each discrete absorber to have a damper that is efficient around the absorber's resonance frequency. It is also important to choose a beam with significant material damping in order to suppress any global low-frequency modes excited by start-up and to have an efficient and fast-responding metamaterial beam absorber.

CONCLUDING REMARKS

This article presents modeling and analysis methods for design of a metamaterial beam consisting of an isotropic beam and small spring-mass-damper subsystems for broadband absorption of transverse elastic waves. Two models of a unit cell are derived and used to demonstrate the existence of a stopband right to the high-frequency side of the local resonance frequency of spring-mass absorbers. A linear finite element method is used for detailed modeling and analysis of simply supported finite beams with different designs of absorbers. We show that the actual working mechanism is that, if the propagating elastic wave's frequency is within the absorbers' stopband, the wave resonates the integrated spring-mass absorbers to vibrate in their optical mode to create shear forces and bending moments to stop the wave propagation. We demonstrate that this unique phenomenon can be used to design broadband absorbers that work for elastic waves of short and long wavelengths. Numerical simulations validate the concept of broadband absorbers and reveal the cause of stopbands. Results show that different distributions of absorbers and their resonance frequencies result in different vibration isolation characteristics. With appropriate design optimization calculations, finite discrete spring-mass absorbers can be used, and hence, expensive micro- or nanomanufacturing techniques are not needed for such

metamaterial beams for broadband vibration absorption/isolation.

ACKNOWLEDGMENT

The first author gratefully acknowledges the financial support of the China Scholarship Council.

REFERENCES

Brillouin, L. 1953. *Wave Propagation in Periodic Structures*, 2nd edn, Dover Publications, New York.

Chen, C. 2005. DARPA Meta-Materials Program Report.

Cheng, Y., Xu, J.Y. and Liu, X.J. 2008. "One-dimensional Structured Ultrasonic Metamaterials With Simultaneously Negative Dynamic Density and Modulus," *Physical Review B*, 77:045134.

Diaz, A.R., Haddow, A.G. and Ma, L. 2005. "Design of Band-gap Grid Structures," *Structural and Multidisciplinary Optimization*, 29:418–431.

Fang, N., Lee, H., Sun, C. and Zhang, X. 2005. "Sub-diffraction-limited Optical Imaging with a Silver Superlens," *Science*, 308:534–537.

Graff, K.F. 1975. *Wave Motion in Elastic Solids*, Dover, New York.

Huang, H.H., Sun, C.T. and Huang, G.L. 2009. "On the Negative Effective Mass Density in Acoustic Metamaterials," *International Journal of Engineering Science*, 47:610–617.

Huang, N.E. and Shen, S.S.P. (eds) 2005. *Hilbert-Huang Transform and Its Applications*, World Scientific Publishing Co., Hackensack, NJ.

Liu, S. 2005. DARPA Meta-Materials Program Report.

Li, J. and Chan, C.T. 2004. "Double-Negative Acoustic Metamaterial," *Physical Review E*, 70:055602(R).

Milton, G.W. and Willis, J.R. 2007. "On Modifications of Newton's Second Law and Linear Continuum Elastodynamics," *Proceedings of the Royal Society of London Series A*, 463:855–880.

Pai, P.F. 2007. Highly Flexible Structures: Modeling, Computation and Experimentation, AIAA, Reston, VA.

Pai, P.F. 2010. "Metamaterial-based Broadband Elastic Wave Absorber," *Journal of Intelligent Material Systems and Structures*, 21:517–528.

Pendry, J.B. 2000. "Negative Refraction Makes a Perfect Lens," *Physical Review Letters*, 85:3966–3969.

Pendry, J.B. 2004. "Negative Refraction," *Contemporary Physics*, 45:191–202.

Pendry, J.B., Schurig, D. and Smith, D.R. 2006. "Controlling Electromagnetic Fields," *Science*, 312:1780–1782.

Sachan, M. and Majetich, S. 2005. DARPA Meta-Materials Program Report.

Schurig, D., Mock, J.J., Justice, B.J., Cummer, S.A., Pendry, J.B., Starr, A.F. and Smith, D.R. 2006. "Metamaterial Electromagnetic Cloak at Microwave Frequencies," *Science*, 314:977–980.

Tanaka, T. 2008. "Plasmonic Metamaterials Produced by Two-photon-induced Photoreduction Technique," *Journal of Laser Micro/Nanoengineering*, 3:152–156.

Tanaka, T., Ishikawa, A. and Kawata, S. 2006. "Unattenuated Light Transmission through the Interface Between Two Materials with Different Indices of Refraction Using Magnetic Metamaterials," *Physical Review B*, 73:125423.

Veselago, V.G. 1968. "The Electrodynamics of Substances with Simultaneously Negative Values of ϵ and μ," *Soviet Physics Uspekhi*, 10:509–514.

Wu, Y., Lai, Y. and Zhang, Z. 2007. "Effective Medium Theory for Elastic Metamaterials in Two Dimensions," *Physical Review B*, 76:205313.

Yao, S., Zhou, X. and Hu, G. 2008. "Experimental Study on Negative Effective Mass in a 1D Mass-Spring System," *New Journal of Physics*, 10:043020.